The $\dot{M}$–$M_{\rm disk}$ Relationship for Herbig Ae/Be Stars: A Lifetime Problem for Disks with Low Masses?

Sierra L. Grant[1] , Lucas M. Stapper[2] , Michiel R. Hogerheijde[2,3] , Ewine F. van Dishoeck[1,2] , Sean Brittain[4] , and Miguel Vioque[5,6]

[1] Max-Planck Institut für Extraterrestrische Physik (MPE), Giessenbachstr. 1, D-85748, Garching, Germany; sierrag@mpe.mpg.de
[2] Leiden Observatory, Leiden University, 2300 RA Leiden, The Netherlands
[3] Anton Pannekoek Institute for Astronomy, University of Amsterdam, The Netherlands
[4] Clemson University, 118 Kinard Laboratory, Clemson, SC 29631, USA
[5] Joint ALMA Observatory, Alonso de Córdova 3107, Vitacura, Santiago 763-0355, Chile
[6] National Radio Astronomy Observatory, 520 Edgemont Road, Charlottesville, VA 22903, USA

Abstract

The accretion of material from protoplanetary disks onto their central stars is a fundamental process in the evolution of these systems and a key diagnostic in constraining the disk lifetime. We analyze the relationship between the stellar accretion rate and the disk mass in 32 intermediate-mass Herbig Ae/Be systems and compare them to their lower-mass counterparts, T Tauri stars. We find that the $\dot{M}$–$M_{\rm disk}$ relationship for Herbig Ae/Be stars is largely flat at $\sim 10^{-7}\ M_\odot\ \mathrm{yr}^{-1}$ over 3 orders of magnitude in dust mass. While most of the sample follows the T Tauri trend, a subset of objects with high accretion rates and low dust masses are identified. These outliers (12 out of 32 sources) have an inferred disk lifetime of less than 0.01 Myr and are dominated by objects with low infrared excess. This outlier sample is likely identified in part by the bias in classifying Herbig Ae/Be stars, which requires evidence of accretion that can only be reliably measured above a rate of $\sim 10^{-9}\ M_\odot\ \mathrm{yr}^{-1}$ for these spectral types. If the disk masses are not underestimated and the accretion rates are not overestimated, this implies that these disks may be on the verge of dispersal, which may be due to efficient radial drift of material or outer disk depletion by photoevaporation and/or truncation by companions. This outlier sample likely represents a small subset of the larger young, intermediate-mass stellar population, the majority of which would have already stopped accreting and cleared their disks.

Unified Astronomy Thesaurus concepts: Pre-main sequence stars (1290); Circumstellar disks (235); Herbig Ae/Be stars (723); Protoplanetary disks (1300)

1. Introduction

Circumstellar disks are the birthplaces of planets, and those planets must form in the first several million years of the disk lifetime before the disk dissipates. It is then important to understand how disks evolve and characterize how that evolution impacts planet formation, and vice versa. The rate at which material is being accreted onto the star from the disk and the disk mass are two key parameters in assessing the evolutionary state of a system. These two diagnostics probe different regions in the disk: the accretion rate traces the innermost star–disk connection, and the disk mass traces the mass reservoir at tens to hundreds of au.

Despite the contrasting scales that the accretion rate ($\dot{M}$) and disk mass ($M_{\rm disk}$) probe, it has been predicted that the two quantities should be related and can give an estimate of the disk lifetime, $t_{\rm disk} = M_{\rm disk}/\dot{M}$ (e.g., Hartmann et al. 1998; Jones et al. 2012; Lodato et al. 2017; Rosotti et al. 2017; Sellek et al. 2020; Manara et al. 2023). The transfer of material inward from the outer disk can be affected by a variety of factors, including the formation of pressure traps, stellar irradiation and photoevaporation, MHD disk winds, and the presence of giant planets and companions (e.g., Jones et al. 2012; Rosotti et al. 2017; Tabone et al. 2022; Zagaria et al. 2022). Deviations from

the nominal $\dot{M}$–$M_{\rm disk}$ relationship can then indicate the presence of one or more of these processes.

Recent observational efforts conducted at optical and near-infrared wavelengths paired with the numerous outer disk surveys, particularly the Atacama Large Millimeter/submillimeter Array (ALMA), have led to large populations of disks with both $\dot{M}$ and $M_{\rm dust}$ measurements (Mendigutía et al. 2012; Manara et al. 2016, 2020; Ansdell et al. 2017; Mulders et al. 2017; Grant et al. 2021; Fiorellino et al. 2022; Testi et al. 2022). However, these surveys have greatly favored low-mass T Tauri stars, with the exception of Mendigutía et al. (2012), which was carried out before ALMA was operational. The more massive Herbig Ae/Be stars, by comparison, lack homogeneous (sub)millimeter observations (Stapper et al. 2022), while they are well covered in surveys focusing on accretion signatures (e.g., Donehew & Brittain 2011; Fairlamb et al. 2015, 2017; Grant et al. 2022; Vioque et al. 2022). The disks around these intermediate-mass stars are thought to form giant exoplanets more efficiently than low-mass stars (Johnson et al. 2010; Reffert et al. 2015). Indeed, van der Marel & Mulders (2021) used disk properties to tentatively point to a connection between stellar mass and giant planet formation. Therefore, it is essential to understand disk evolution and planet formation in the disks around intermediate-mass stars. In this work, we take these two key disk diagnostics, $\dot{M}$ and $M_{\rm disk}$, to study the $\dot{M}$–$M_{\rm disk}$ relationship in a sample of 32 Herbig Ae/Be objects.

Table 1
Properties of Our Sample

Source	R.A.	Decl.	M_* $(M_\odot)$	$\log_{10}(L_*)$ $(L_\odot)$	Age (Myr)	$\log_{10}(\dot{M})$ $(M_\odot\ \mathrm{yr}^{-1})$	M_{dust} $(M_\oplus)$	Group	Binary
AB Aur	04:55:45.9	+30:33:04	$2.152^{+0.359}_{-0.214}$	$1.61^{+0.19}_{-0.21}$	$4.05^{+1.43}_{-1.49}$	-6.13 ± 0.27 (a)	11.8 ± 1.2	I	Yes
AK Sco	16:54:44.8	−36:53:19	$1.401^{+0.070}_{-0.070}$	$0.62^{+0.03}_{-0.01}$	$8.382^{+1.72}_{-0.42}$	<-8.06	6.1 ± 0.6	II	Yes
BF Ori	05:37:13.3	−06:35:01	$1.807^{+0.090}_{-0.090}$	$1.29^{+0.06}_{-0.05}$	$6.38^{+0.32}_{-0.46}$	-7.28 ± 0.39	1.1 ± 0.1	II	
CQ Tau	05:35:58.5	+24:44:54	$1.468^{+0.189}_{-0.109}$	$0.87^{+0.18}_{-0.12}$	$8.898^{+2.80}_{-2.52}$	<-8.33	44.2 ± 4.8	I	Yes
HD 100453	11:33:05.5	−54:19:29	$1.251^{+0.063}_{-0.063}$	$0.79^{+0.02}_{-0.00}$	$6.528^{+0.45}_{-0.49}$	-8.32 ± 0.51	17.5 ± 1.8	I	Yes
HD 100546	11:33:25.3	−70:11:41	$2.055^{+0.103}_{-0.123}$	$1.37^{+0.07}_{-0.05}$	$5.48^{+1.41}_{-0.77}$	-6.95 ± 0.36	38 ± 3.9	I	
HD 104237	12:00:04.9	−78:11:35	$1.849^{+0.092}_{-0.092}$	$1.33^{+0.04}_{-0.01}$	$5.48^{+0.27}_{-0.4}$	-6.43 ± 0.34	10.5 ± 1.1	II	Yes
HD 135344B	15:15:48.4	−37:09:16	$1.432^{+0.072}_{-0.072}$	$0.79^{+0.03}_{-0.04}$	$8.927^{+0.45}_{-0.91}$	<-8.15	35.2 ± 3.8	I	Yes
HD 139614	15:40:46.4	−42:29:54	$1.481^{+0.074}_{-0.074}$	$0.77^{+0.03}_{-0.01}$	$14.49^{+1.41}_{-3.60}$	-8.14 ± 1.03	41.7 ± 4.3	I	
HD 141569	15:49:57.7	−03:55:17	$1.860^{+0.093}_{-0.093}$	$1.22^{+0.03}_{-0.03}$	$8.616^{+11.38}_{-1.19}$	-7.76 ± 0.65	0.36 ± 0.04	II	Yes
HD 142527	15:56:41.9	−42:19:24	$1.613^{+0.124}_{-0.081}$	$0.96^{+0.03}_{-0.00}$	$6.627^{+0.33}_{-1.55}$	<-7.29	214.9 ± 22.1	I	Yes
HD 142666	15:56:40.0	−22:01:40	$1.493^{+0.075}_{-0.075}$	$0.94^{+0.04}_{-0.05}$	$9.33^{+0.77}_{-0.47}$	-7.63 ± 1.26	25.1 ± 2.6	II	
HD 163296	17:56:21.3	−21:57:22	$1.833^{+0.092}_{-0.092}$	$1.20^{+0.06}_{-0.03}$	$7.598^{+1.05}_{-1.22}$	-7.27 ± 0.75	46.7 ± 5	II	
HD 169142	18:24:29.8	−29:46:50	$2.000^{+0.131}_{-0.128}$	$1.31^{+0.12}_{-0.12}$	$8.984^{+11.02}_{-3.90}$	-7.09 ± 0.21 (a)	22.9 ± 2.4	I (b)	
HD 176386	19:01:38.9	−36:53:27	$2.299^{+0.143}_{-0.299}$	$1.58^{+0.12}_{-0.22}$	$4.05^{+15.95}_{-0.57}$	-7.08 ± 0.2 (a)	<0.06	II (c)	Yes
HD 245185	05:35:09.6	+10:01:51	$1.923^{+0.177}_{-0.096}$	$1.29^{+0.13}_{-0.10}$	$7.643^{+12.36}_{-2.56}$	-6.85 ± 0.36	41.5 ± 7.6	I	Yes
HD 290764	05:38:05.3	−01:15:22	$1.691^{+0.128}_{-0.085}$	$1.18^{+0.09}_{-0.09}$	$6.89^{+0.54}_{-1.41}$	-7.0 ± 0.39	90.3 ± 11.8	I	
HD 31648	04:58:46.3	+29:50:37	$1.779^{+0.131}_{-0.089}$	$1.27^{+0.14}_{-0.05}$	$6.201^{+0.31}_{-1.12}$	-6.57 ± 0.17 (a)	70.9 ± 7.7	II (b)	
HD 34282	05:16:00.5	−09:48:35	$1.450^{+0.072}_{-0.072}$	$0.98^{+0.05}_{-0.04}$	$6.54^{+2.41}_{-0.63}$	-7.5 ± 0.73	86.8 ± 9.7	I	Yes
HD 36112	05:30:27.5	+19:25:57	$1.564^{+0.108}_{-0.078}$	$1.04^{+0.12}_{-0.08}$	$8.289^{+0.41}_{-1.40}$	-7.32 ± 0.4	18.8 ± 2	I	Yes
HD 37258	05:36:59.3	−06:09:16	$1.881^{+0.136}_{-0.108}$	$1.24^{+0.12}_{-0.10}$	$7.929^{+12.07}_{-2.45}$	-6.98 ± 0.37	2.4 ± 0.4	II	Yes
HD 53367	07:04:25.5	−10:27:16	12^{+4}_{-}	$3.13^{+0.23}_{-0.17}$	$0.08^{+0.08}_{-0.08}$	-6.97 ± 0.45	<0.05	I	Yes
HD 58647	07:25:56.1	−14:10:44	$3.867^{+0.333}_{-0.193}$	$2.44^{+0.11}_{-0.09}$	$0.8372^{+0.12}_{-0.18}$	-5.84 ± 0.31	1 ± 0.1	II	Yes
HD 9672	01:34:37.9	−15:40:35	$1.810^{+0.090}_{-0.090}$	$1.17^{+0.09}_{-0.02}$	$6.89^{+0.34}_{-0.51}$	-7.8 ± 1.0 (a)	0.13 ± 0.01	II (b)	
HD 97048	11:08:03.2	−77:39:17	$2.252^{+0.113}_{-0.135}$	$1.54^{+0.07}_{-0.06}$	$4.37^{+1.11}_{-0.32}$	-6.49 ± 0.34	155.9 ± 16	I	Yes
HR 5999	16:08:34.3	−39:06:19	$2.432^{+0.122}_{-0.122}$	$1.72^{+0.05}_{-0.04}$	$2.729^{+0.26}_{-0.35}$	-6.0 ± 0.11 (a)	4 ± 0.4	II (b)	Yes
MWC 297	18:27:39.5	−03:49:52	$16.901^{+1.868}_{-1.215}$	$4.59^{+0.12}_{-0.12}$	$0.02754^{+0.006}_{-0.006}$	<-5.89	65.7 ± 9.6	I	Yes
TY CrA	19:01:40.8	−36:52:34	$2.063^{+0.223}_{-0.190}$	$1.41^{+0.14}_{-0.23}$	$6.38^{+13.62}_{-2.01}$	<-8.31 (d)	0.10 ± 0.01	I (b)	Yes
V1787 Ori	05:38:09.3	−06:49:17	$1.659^{+0.094}_{-0.083}$	$1.15^{+0.11}_{-0.09}$	$7.43^{+0.59}_{-1.05}$	-7.17 ± 0.38	24.2 ± 2.9	II	
V599 Ori	05:38:58.6	−07:16:46	$2.029^{+0.101}_{-0.101}$	$1.44^{+0.06}_{-0.06}$	$4.289^{+0.42}_{-0.54}$	-6.71 ± 0.37	75 ± 8.6	I	
V718 Sco	16:13:11.6	−22:29:07	$1.605^{+0.080}_{-0.080}$	$0.90^{+0.05}_{-0.04}$	$9.804^{+2.80}_{-0.49}$	-7.49 ± 0.23 (a)	11.9 ± 1.3	II (b)	Yes
VV Ser	18:28:47.9	+00:08:40	$2.892^{+0.145}_{-0.145}$	$1.95^{+0.10}_{-0.08}$	$2.77^{+8.13}_{-0.21}$	<-6.14	2.3 ± 0.3	II	

Note. Accretion rates with (a) come from Wichittanakom et al. (2020), (d) come from Garcia Lopez et al. (2006), and the rest are from Grant et al. (2022). Groups marked with (b) are from Guzmán-Díaz et al. (2021), (c) are from Boersma et al. (2009), and the rest are from Grant et al. (2022). Dust masses are from Stapper et al. (2022). Binary information is from the compilation in Vioque et al. (2018).

## 2. Sample, Mass Accretion Rates, and Dust Masses

2.1. Sample

Our sample is compiled from the ALMA-observed sample of Stapper et al. (2022), which provides the dust masses used in this work. Their sample consists of the Herbig Ae/Be systems in Vioque et al. (2018) that are within 450 pc and had available ALMA observations (see Stapper et al. 2022 for more details and notes on some excluded objects).

The stellar properties for our sample are listed in Table 1 and largely from Vioque et al. (2018). Thirty-one of our 32 sources have high-quality Gaia DR2 parallaxes that were used in Vioque et al. (2018), which are largely consistent with Gaia (E) DR3 (Guzmán-Díaz et al. 2021). One source, HD 53367, was in the low-quality sample, and the Gaia DR3 parallax is very different from that of DR2 (parallax of 0.8199 ± 0.2114 mas in DR3 and 7.7682 ± 0.7854 mas in DR2). We keep this source in our sample using the stellar parameters based on the Gaia DR2 data, but we urge caution in interpreting the results for this source, and we do not include it in fits to the $\dot{M}-M_{\mathrm{disk}}$ relationship that we present in Section 3. The stellar masses

range from 1.3 to 16.9 $M_\odot$, but 29 of our 32 sources have stellar masses of less than 3 $M_\odot$. Our sample represents a slightly older population, with 27 of our sources having ages greater than 3 Myr. The Meeus et al. (2001) group determinations, which are determined from the spectral energy distributions (SEDs) and thought to reflect the dust disk structure (e.g., Meeus et al. 2001; van Boekel et al. 2005; Maaskant et al. 2013; Garufi et al. 2017; Stapper et al. 2022), are largely from the SED analysis of Guzmán-Díaz et al. (2021) and Grant et al. (2022). Our sample is nearly evenly split between group I (17) and group II (15) disks.

2.2. Mass Accretion Rates

The accretion rates for our sample come from the works of Garcia Lopez et al. (2006), Wichittanakom et al. (2020), and Grant et al. (2022). Grant et al. (2022) used Brγ observations to derive $L_{\mathrm{Br}\gamma}$, which was then converted to an accretion luminosity using the relationship from Fairlamb et al. (2017). Similarly, Wichittanakom et al. (2020) did the same, except using Hα instead of Brγ. The Hα and Brγ have a similar spread
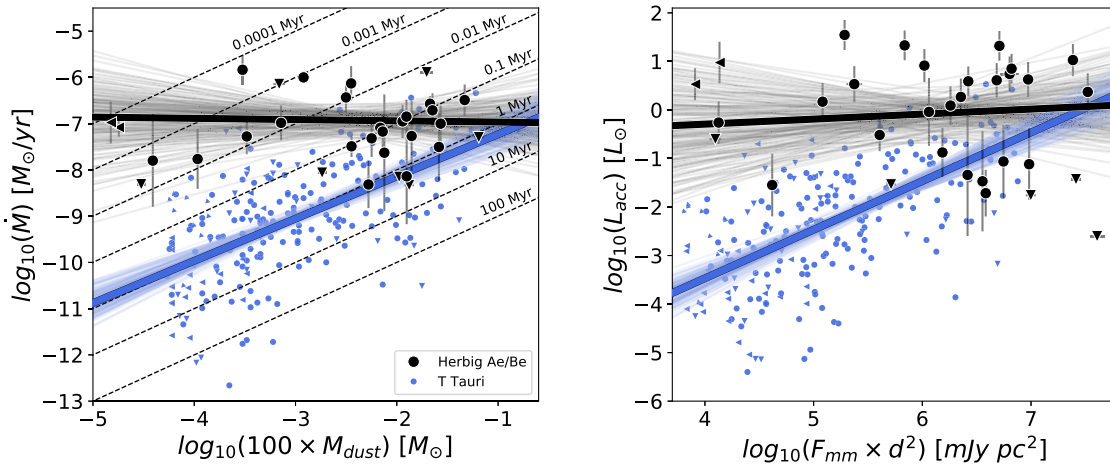
Figure 1. Left: $\dot{M}-M_{\mathrm{disk}}$ relationship for our sample of Herbig Ae/Be stars (black points) and the T Tauri stars from Testi et al. (2022; blue points). We have excluded the few sources in the Testi et al. (2022) sample that have $M_* > 1.5\, M_\odot$. The black line is the best fit for the Herbig Ae/Be sample, and the blue line is the best fit for the T Tauri sample. The thin black and blue lines are 200 samples of the posterior for the fits to the Herbig Ae/Be and T Tauri points, respectively. Upper limits on the dust mass are shown as leftward-facing triangles, and upper limits on the accretion rate are shown as downward-facing triangles. If both the accretion rate and dust mass measurements are upper limits, the triangle points to the lower left. The dotted gray lines show different disk lifetimes. The Herbig Ae/Be disks are outliers above the already large scatter seen for the lower-mass stars. Right: relationship between the accretion luminosity and the millimeter flux (normalized by the distance).

in the empirical relationship between L_{line} and L_{acc} and are both robust tracers of accretion, even if the line is not generated in the accretion columns (e.g., Mendigutía et al. 2015). For one object, TY CrA, we use the accretion rate from Garcia Lopez et al. (2006). For this target, the Brγ line is in absorption that is mostly consistent with the photosphere; therefore, there is only an upper limit on the accretion rate, and we do not include it in the $\dot{M}-M_{\mathrm{disk}}$ fits that we discuss in the rest of the paper.

The median accretion rate in our sample is $\log_{10}(\dot{M}) = -7.09$ ($M_\odot\,\mathrm{yr}^{-1}$), not including upper limits, with a median log error of 0.37. Both sources of the accretion rate measurements rely on the assumption that magnetospheric accretion is the dominant mechanism in these sources. However, the Herbig Ae/Be stellar mass/effective temperature range is thought to be the regime where magnetospheric accretion may break down to boundary layer accretion due to the weak stellar magnetic fields (e.g., Vink et al. 2002; Donehew & Brittain 2011; Mendigutía et al. 2011; Cauley & Johns-Krull 2014; Wichittanakom et al. 2020; Grant et al. 2022). Based on the findings of Wichittanakom et al. (2020), Grant et al. (2022), and Vioque et al. (2022), the accretion mechanism change may occur at the $\sim 4\, M_\odot$ boundary, and only two stars in our sample are above this boundary, HD 53367 and MWC 297.

We have no targets with an accretion rate detection below $10^{-9}\, M_\odot\,\mathrm{yr}^{-1}$. One of the criteria needed for Herbig Ae/Be classification is the presence of an accretion tracer, frequently H I lines in emission (e.g., Herbig 1960; The et al. 1994). The use of these lines in identifying Herbig Ae/Be stars is complicated by the fact that these stars have photospheric absorption at those lines and that the depth of the photospheric absorption depends on the stellar effective temperature (Joner & Hintz 2015; Fairlamb et al. 2017). The lower limit on the detectable accretion rate varies with spectral type, the ability to characterize the photosphere, and the measurement method. For example, the lower limit on the measurement of the accretion rate from the veiling of the Balmer jump in the near-ultraviolet (NUV) ranges from a few times $10^{-9}\, M_\odot\,\mathrm{yr}^{-1}$ for $2\, M_\odot$ Herbig stars to about $10^{-6}\, M_\odot\,\mathrm{yr}^{-1}$ for $7\, M_\odot$ Herbig stars

(see Figure 5 in Sicilia-Aguilar et al. 2016). If one assumes that the calibration of line and accretion luminosity inferred from the NUV excess is valid for lower accretion rates, then it is possible to infer lower levels of accretion from spectroscopy of those lines. Fairlamb et al. (2015) also highlighted the changing lower accretion limits based on stellar effective temperature (see their Figure 9). From Sicilia-Aguilar et al. (2016) and Fairlamb et al. (2015), an accretion rate of $\sim 10^{-9}\, M_\odot\,\mathrm{yr}^{-1}$ is generally the lower limit for the lowest stellar mass objects in the Herbig Ae/Be classification. The accretion rate values in this work are all above this level, including the outlier objects that are discussed in Section 3. We discuss the lack of low accretion rate objects in more detail in Section 4.2.

2.3. Dust Masses

The dust masses in this work were determined in Stapper et al. (2022) using archival ALMA observations. The spatial resolution in these observations ranges from 0″02 to 1″84. Our sample is evenly split between resolved and unresolved disks, although more group I disks are resolved (11/17) than group II (5/15). The average spatial resolution for the group I disks is 0″37, while the average is 0″88 for the group II disks. The disk-integrated millimeter fluxes were converted to dust masses using a dust temperature that is scaled by the stellar luminosity (Andrews et al. 2013). The adopted dust opacities, κ_ν, were determined by a power law such that $\kappa_\nu = 10\,\mathrm{cm}^2\,\mathrm{g}^{-1}$ at 1000 GHz (Beckwith et al. 1990) and scales with an index of 1. In this work, we assume that the disk mass is 100 times the dust mass; however, we discuss the implications of this assumption in Section 4.1.

3. Results

The $\dot{M}-M_{\mathrm{disk}}$ relationship for our Herbig Ae/Be sample is presented in Figure 1. We fit the Herbig Ae/Be $\dot{M}-M_{\mathrm{disk}}$ relationship using the method from Kelly (2007),[7] taking errors on $\dot{M}$ and M_{disk} and upper limits into account (Fiorellino et al. 2022; Testi et al. 2022). We find that the $\dot{M}-M_{\mathrm{disk}}$

---

[7] https://linmix.readthedocs.io
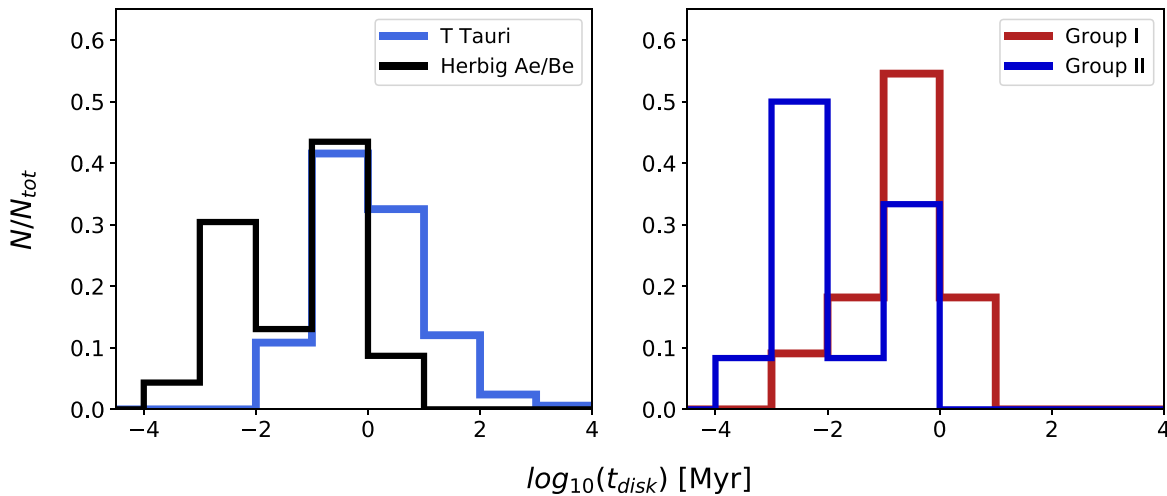
Figure 2. Left: t_{disk} distribution for T Tauri disks from Testi et al. (2022; blue) and our Herbig Ae/Be sample (black). We have removed any targets from the Testi et al. (2022) sample that have $M_* > 1.5\,M_\odot$. Objects with upper limits on $\dot{M}$ or M_{disk} are not included. A two-sample Kolmogorov–Smirnov test returns a p-value of 2.7×10^{-7}, indicating that the distributions are drawn from different populations. Right: t_{disk} distribution for group I (red) and group II (blue) disks. A two-sample Kolmogorov–Smirnov test returns a p-value of 0.02, indicating that the distributions may be drawn from different populations.

relationship in our Herbig Ae/Be sample is $\log_{10}(\dot{M}) = (-0.03 \pm 0.21)\log_{10}(M_{\mathrm{disk}}) + (-6.99 \pm 0.52)$, a mostly flat relationship over 3 orders of magnitude in dust mass. This $\dot{M}$–M_{disk} relationship is drastically different from that of low-mass systems, in particular the large sample compiled and analyzed by Testi et al. (2022; Figure 1). At the highest disk masses, the Herbig Ae/Be sample largely overlaps with the T Tauri population, although at the higher end of the accretion rate range. However, at the low disk mass end, the Herbig Ae/Be objects lie at and well above the upper end of the T Tauri star accretion rate distribution. The flat relationship that we find for our sample is likely influenced by the fact that Herbig Ae/Be stars require accretion signatures to be classified as such, and accretion generally cannot be measured below $\sim 10^{-9}\,M_\odot\,\mathrm{yr}^{-1}$ in intermediate-mass stars. Therefore, we lack objects with low accretion rates that may steepen the relationship for intermediate-mass stars in general. While this lower limit is important to keep in mind when interpreting the Herbig Ae/Be $\dot{M}$–M_{disk} relationship, the flatness of the observed relationship highlights the objects with high accretion rates and low dust masses as clear outliers.

Also shown in Figure 1 is the relationship between the accretion luminosity and the millimeter flux (normalized by the distance), and the same flat trend is present for the Herbig Ae/Be stars, while the T Tauri stars again show a steeper relationship. The fact that these more "direct" quantities show the same relationship indicates that any assumptions going into the determination of the accretion rate and disk mass (e.g., the dust temperature, magnetospheric accretion being the only source of emission used in determining the accretion rates, etc.) are not the root cause of the flat $\dot{M}$–M_{disk} relationship for the Herbig Ae/Be sample.

The inferred disk lifetime, $t_{\mathrm{disk}} = M_{\mathrm{disk}}/\dot{M}$, is a good measure of how much a given disk deviates from the relationship seen for the T Tauri disks, which cluster around the $t_{\mathrm{disk}} \sim 1$ Myr line. The low disk mass objects in our sample have accretion rates that indicate that the disk will be depleted on much shorter timescales, with 12 of our 32 disks having inferred disk lifetimes of less than 10,000 yr (0.01 Myr). We show the distribution of t_{disk} in Figure 2, comparing the T Tauri

sample of Testi et al. (2022) to our sample of Herbig Ae/Be sources. A two-sample Kolmogorov–Smirnov test (Virtanen et al. 2020) returns a p-value of 2.7×10^{-7}, indicating that the T Tauri and Herbig Ae/Be samples are drawn from different populations. Figure 2 also shows the Herbig Ae/Be distribution when broken into group I and group II sources, showing that the group II sources are clearly bimodal, while the group I distribution is unimodal. A two-sample Kolmogorov–Smirnov test (Virtanen et al. 2020) returns a p-value of 0.02, indicating that the distributions may be drawn from different populations. We show the $\dot{M}$–M_{disk} relationship broken up into group I and group II objects in Figure 3.

In the Appendix, we discuss each of the 12 low disk mass sources that stand out in the $\dot{M}$–M_{disk} relationship. In particular, we compare our $\dot{M}$ and M_{disk} values to previous values in the literature. We find that our accretion rate values are consistent with those in the literature, subject to differences in accretion determination and variability. In contrast, our disk masses tend to be lower due to a combination of higher-resolution observations, which reduce the amount of contamination from nearby sources/cloud emission, and higher dust temperatures. For instance, this population of high accretion rate, low disk mass objects was not seen in the $\dot{M}$–M_{disk} analysis of Mendigutía et al. (2012), which found that the $\dot{M}$–M_{disk} relationship for Herbig Ae/Be stars was in line with that of the T Tauri stars. Nine of our objects overlap with their sample, and we have compared the accretion rates and dust masses used in each work. Their accretion rates are within an order of magnitude of ours and evenly split between being higher and lower than our values. The Stapper et al. (2022) disk mass values are lower than those in Mendigutía et al. (2012) in six sources (one has a higher value in our work, one is an upper limit in Mendigutía et al. 2012, and one has no disk mass determination in Mendigutía et al. 2012 due to a lack of millimeter flux). This is due to two differences: (1) the millimeter fluxes from ALMA used by Stapper et al. (2022) are lower in six out of seven targets, likely due to higher angular resolution observations that suffer less from contamination, and (2) higher dust temperatures are used by Stapper et al. (2022). The dust temperatures in Stapper et al. (2022) were determined
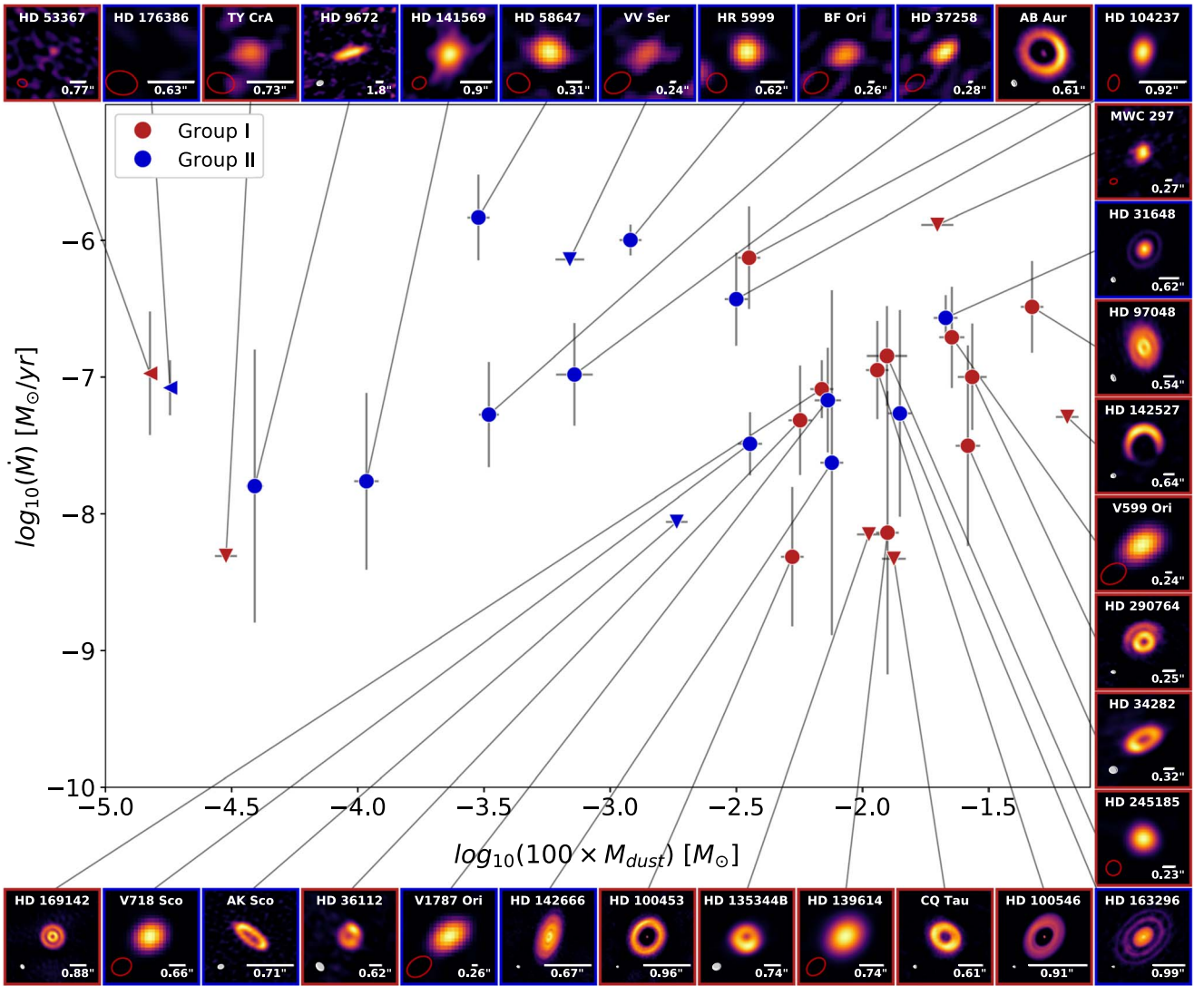
Figure 3. The $\dot{M}-M_{disk}$ relationship for the Herbig Ae/Be stars broken up by group classification (group I sources in red and group II sources in blue). Upper limits are the same as in Figure 1. ALMA continuum images from Stapper et al. (2022) are shown for each object with a 100 au scale bar and the beam at the bottom of each image. If the disk is unresolved in the ALMA observations, the beam is shown in red.

by scaling by the stellar luminosity, while the temperatures in Mendigutía et al. (2012) were determined from graybody fits to photometry at wavelengths longer than 350 μm. We note that if we adopt a uniform dust temperature of 20 K, as is commonly done for lower-mass stars, the disk lifetimes increase but not enough to remove the low inferred disk lifetimes, with all 12 low disk mass sources still having disk lifetimes of less than 0.1 Myr. See the Appendix for further comparison of various disk mass determinations in the literature for these 12 targets.

4. Discussion

In this sample of Herbig Ae/Be objects, we find that the $\dot{M}$ $−M_{disk}$ relationship is relatively flat. While the majority of objects fall along the nominal, steep $\dot{M}−M_{disk}$ relationship of the T Tauri stars, the relationship in our sample is being affected by a subset of objects appearing to have accretion rates inconsistent with their disk masses, such that the disks have a very short inferred lifetime. This outlier sample is likely present due to the biases in Herbig Ae/Be classification, which are limited to objects with accretion rates above $\sim10^{-9} M_{\odot}\,\text{yr}^{-1}$. Here we focus on these short-lifetime "outlier" objects, first, to

discuss factors that would move these targets into the nominal $\dot{M}−M_{disk}$ regime, and second, to explain these targets if their disk masses and accretion rates are not under- and overestimated, respectively.

4.1. Factors that Would Move the Outliers into the General Spread

Here we consider the possibility that either the accretion rates or the dust masses for the low-lifetime objects may be over- and underestimated, respectively.

1. Optical depth. In the scenario where group II disks are undergoing efficient radial drift, the dust disks will be compact and may be optically thick at millimeter wavelengths. which would then lead us to underestimate the dust, and therefore disk, masses (Liu et al. 2022; Stapper et al. 2022). Modeling efforts, paired with observations at centimeter wavelengths that may be optically thin if the millimeter wavelengths are not, are needed to establish if optically thick emission is the cause of the low disk mass determinations. However, based on

the gas masses available for some of these objects (next point), it is unlikely that this is the case for all of these sources.

2. Gas mass. We are inferring a disk mass based on a gas-to-dust mass ratio of 100. If the true gas-to-dust mass ratio is higher, then our "low-mass" disks may be high enough to move the objects to the right enough in the $\dot{M}$–M_{disk} plane to make the relationship more consistent with what is seen for lower-mass stars (e.g., Sellek et al. 2020). Note that the same problem may exist for low-mass stars, even when taking into account the freeze-out of common gas tracers (e.g., Miotello et al. 2023). We find gas mass or gas-to-dust mass ratios available in the literature for 11 of our 32 objects (van der Marel et al. 2016; Boehler et al. 2017; Miley et al. 2018; Yen et al. 2018; Kama et al. 2020; Rivière-Marichalar et al. 2022). Of these, five are upper limits that are above, and therefore consistent with, the disk masses that we use here. There are four objects for which the gas mass or gas-to-dust mass ratios are below the values inferred from the dust continuum. Finally, two objects have gas masses that are above what we assume here, neither of which changes the disk lifetime substantially. Further discussion of gas masses for the low dust mass, high accretion rate objects is given in the Appendix. (Additionally, L. Stapper et al. (2023, in preparation) will provide a detailed analysis of the gas tracers for this sample.) Further careful analysis of gas observations of the disks around Herbig Ae/Be stars is needed to determine the true disk mass, in particular, using gas tracers that are themselves optically thin (Booth et al. 2019). With these gas masses, we would then be able to determine whether the "low-mass" disks are really on the verge of dissipation or whether there is still a large gas reservoir.

3. Disk winds. There is evidence that disk winds contribute to the Brγ line that is largely used to derive the accretion rates in this work (e.g., Kraus et al. 2008; Kurosawa et al. 2016; Hone et al. 2019; Wojtczak et al. 2023). If this is the case, then a given accretion rate used here may be artificially inflated. If we instead take accretion rates determined using ultraviolet observations from Donehew & Brittain (2011), Mendigutía et al. (2011), and Fairlamb et al. (2015), which are unaffected by any contribution from a disk wind, the mismatch in slope between the T Tauri stars and Herbig Ae/Be objects is even larger. For example, Mendigutía et al. (2011) used the Balmer discontinuity and found an accretion rate of $1.45 \times 10^{-5}\ M_\odot\ \mathrm{yr}^{-1}$ for HD 58647, a factor of 10 higher than the value we use that was determined from Brγ. On the other hand, Brittain et al. (2007) found an accretion rate of $3.5 \times 10^{-7}\ M_\odot\ \mathrm{yr}^{-1}$ using Brγ. Despite the discrepancies in the accretion rate, none of these values solve the short lifetime implied for this disk, which has a dust mass of $1 \pm 0.1\ M_\oplus$. With the Brittain et al. (2007) accretion rate, the disk lifetime is 860 yr; with the Grant et al. (2022) accretion rate adopted here, it is 206 yr; and with the Balmer discontinuity accretion rate from Mendigutía et al. (2011), it is only 21 yr.

To summarize, if all of the outlier group II disks are extremely optically thick, have gas-to-dust ratios that are much larger than the standard interstellar medium value of 100, or have disk winds that contribute significantly to the accretion

tracers used to determine the accretion rate, these objects could really be in the nominal disk lifetime regime. While this needs to be investigated further, literature values of the gas mass and accretion rates determined from ultraviolet observations, which do not suffer from contributions from disk winds, indicate that the trends we are seeing are robust.

4.2. Making Sense of the Outliers

If the mass accretion rates, dust masses, and gas-to-dust ratios are not wildly off due to the factors discussed above, how might we explain this low-lifetime population of disks? Either these sources are rapidly depleting their disks and we are observing them just as they are about to dissipate, or we are witnessing these sources undergoing variable accretion and happen to be catching them at a point of high accretion that will then decrease before the disk is fully dissipated. We explore these options here.

The low disk lifetime objects are predominantly group II disks. Our understanding of what these group classifications means has evolved significantly with additional observations and analysis since the classification by Meeus et al. (2001). Maaskant et al. (2013), Garufi et al. (2017), and Stapper et al. (2022) all found evidence for large cavities in the disks of group I objects. Additionally, Stapper et al. (2022) found that the group I disks have higher dust masses than the group II disks, with the group II disks potentially unable to form giant planets at large radii, resulting in efficient radial drift and compact disks. This agrees with the interpretation of Kama et al. (2015) and Guzmán-Díaz et al. (2023), who found that refractory elements were depleted in the photospheres of group I objects relative to group II disks, suggesting dust trapping in group I disks by giant planets. The dust mass difference is the source of the difference in the $\dot{M}$–M_{disk} relationship, as the accretion rates have been found to be consistent between group I and II systems (Mendigutía et al. 2012; Banzatti et al. 2018; Grant et al. 2022).

If we apply the interpretations of group I and II disks as being gapped and potentially hosting giant planets at large radii versus being unable to form giant planets at large radii and thus having radially compact disks, then the difference in the $\dot{M}$–M_{disk} relationship becomes clearer (Figure 3). In this scenario, group I disks form giant planets, clearing large gaps in the gas and dust, and are surrounded by dust rings at large radii (see the ALMA continuum images in Figure 3). If group II disks are not able to form giant planets, then they are unable to trap gas or dust in the outer disk, resulting in a rapid inflow of material to the inner disk, which maintains a high accretion rate. It is unclear when these systems will then begin to decrease in accretion rate and how rapid that decrease is. This would result in radially compact dust disks for the group II sources, but higher-resolution observations are needed to confirm, as none of the low disk lifetime ($<0.01\ \mathrm{Myr}$) group II disks are currently resolved (Figure 3). The group II disks have an average spatial resolution in the ALMA observations of $0\rlap{.}{''}88$, compared to $0\rlap{.}{''}37$ for the group I disks. Additionally, comparing the gas and dust radii will be crucial for determining if efficient radial drift can explain these systems (e.g., Trapman et al. 2019; Toci et al. 2021).

Other factors that can result in the low disk masses for these objects could come from outer disk depletion from photo-evaporation and/or be due to multiplicity. If these objects are close to nearby massive stars, the extreme irradiation

environments can strip away material, leaving the outer disk depleted (e.g., Mann et al. 2014; Ansdell et al. 2017; Eisner et al. 2018; Winter et al. 2018). Multiplicity has also been shown to impact outer disk evolution, resulting in truncation of the disk (Manara et al. 2019; Panić et al. 2021; Zagaria et al. 2022). If any companions are massive stars themselves, then these disks may doubly suffer from truncation and photoevaporation.

Twenty of the 32 objects in our sample are known binaries; however, the fraction could be higher given the limited surveys that have searched for multiple systems. To identify the binaries in this sample, we use the binary information from Vioque et al. (2018), largely collected from Leinert et al. (1997), Baines et al. (2006), and Wheelwright et al. (2010). There are two interesting examples in our sample to study the effects of multiplicity and photoevaporation: the TY CrA/HD 176386 and HR 5999/HR 6000 systems. Object TY CrA is in a close triple, if not quadruple, system (e.g., Vaňko et al. 2013) and close to HD 176386, another target in our sample that has a low inferred disk lifetime and is also a binary. The second example comes from HR 5999, which is itself a binary and 45″ (∼7000 au at a distance of 158 pc) to HR 6000, an early A-type star with no evidence of a disk (Stelzer et al. 2009). The low disk masses of these systems may be due to photoevaporation and/or truncation from their companions. High spatial resolution observations in both the gas and dust, paired with photoevaporation and dynamic truncation models (e.g., Rosotti & Clarke 2018), will help to distinguish the effects of binarity and photoevaporation in these multiple systems.

If these disks are on the verge of dissipation, why do we see them at all? Either these disks are going through an accretion outburst such that, despite their low disk masses, we are still able to classify them as Herbig Ae/Be stars, or these high accretion rate, low disk mass objects make up only a small portion of the young, intermediate-mass young stellar object population.

The fact that low-$\dot{M}$ targets are not in our sample is not surprising; Herbig Ae/Be stars are, in part, identified due to the presence of accretion-tracing lines, namely, H I lines in emission (e.g., Herbig 1960; The et al. 1994). In practice, only a handful of Herbig Ae/Be stars have rates lower than $1 \times 10^{-8} M_{\odot} \, yr^{-1}$ (7/267 in the sample of Vioque et al. 2022, 10/102 in the sample of Grant et al. 2022). Mooley et al. (2013) searched for such objects in the Taurus star-forming region. They identified three B-type stars and two A-type stars that are probable members. They also identified two other stars that are plausible members. Thus, half of the A and B stars in this star-forming region do not show obvious signatures of accretion. Iglesias et al. (2023) used a volume-limited sample (out to 300 pc) and found that only six out of 134 targets in their sample of young, intermediate-mass stars ($1.5 \, M_{\odot} \leqslant M_* \leqslant 3.5 \, M_{\odot}$) show the accretion signatures needed to designate them as Herbig Ae/Be stars. These results suggest that there is a significant population of A and B stars in our volume (out to 450 pc) that are analogous to the weak-lined T Tauri stars. Therefore, the sample of Herbig Ae/Be objects studied in this work may not be representative of the intermediate-mass young stellar object population as a whole, with most of these objects already having dissipated their disks and thus not meeting the criteria for Herbig Ae/Be objects. Despite this bias, HD 9672 (49 Cet) in our sample is potentially at an intermediate stage, as it has been characterized in different works as a debris disk

(Zuckerman & Song 2012), albeit one with a large CO gas content (e.g., Moór et al. 2019; Higuchi et al. 2020), and as a Herbig Ae system (Vioque et al. 2018). Similarly, HD 141569 in our sample has been considered a "hybrid" disk in the transition phase between a protoplanetary disk and a debris disk (Augereau & Papaloizou 2004; Miley et al. 2018; Di Folco et al. 2020; Gravity Collaboration et al. 2021; Iglesias et al. 2023). These targets may represent the bridge between protoplanetary and debris disks.

The short disk lifetimes inferred in this work have relied on the assumption that the accretion rate is constant in time. However, young stars are known to be variable, with wide-ranging timescales for variability (see the recent review by Fischer et al. 2023). If these low-lifetime targets are undergoing a period of high accretion that will not last, then the disks may not deplete on the short timescales inferred. This has been seen to impact T Tauri stars (Claes et al. 2022); however, this variability may not be enough to explain the spread in the accretion rates measured for T Tauri stars (Manara et al. 2023). How this variability might be different for higher-mass objects, if it is different at all, is unclear (see the discussion on this topic for Herbig Ae/Be objects in Brittain et al. 2023). Characterizing variability in Herbig Ae/Be objects and putting them into context with young, diskless A and B stars will be crucial for determining whether the low-lifetime population seen here is simply a subset of the larger population that is undergoing periods of strong accretion and thus included in Herbig Ae/Be samples.

5. Summary and Conclusions

We analyze a sample of 32 Herbig Ae/Be objects (1.3–16.9 $M_{\odot}$) to determine the relationship between the accretion rate and the dust disk masses. We find the following.

1. The mass accretion rate is roughly constant with disk mass, as probed by the dust mass, for Herbig Ae/Be stars ($\dot{M} \sim 10^{-7} M_{\odot} \, yr^{-1}$). This is significantly different from the steeper relationship found for T Tauri stars, likely due in part to the biases in classifying stars as Herbig Ae/Bes. While ∼two-thirds of the sample follows the $\dot{M}$–M_{disk} relationship of the T Tauri stars, one-third has high accretion rates relative to their dust masses.

2. The T Tauri stars and Herbig Ae/Be systems show very different disk lifetime ($t_{disk} = M_{disk}/\dot{M}$) distributions, with ∼30%–40% of the Herbig Ae/Be sample having disk lifetimes shorter than 0.01 Myr, with this population being dominated by group II disks (identified by low infrared excesses).

3. If the disk masses are underestimated (due to optical depth effects or a higher-than-expected gas-to-dust mass ratio) or the accretion rates are overestimated (due to contributions to the accretion tracers by winds), the outlier objects may actually reside in the nominal $\dot{M}$–M_{disk} relationship. However, based on values of the disk gas mass measurements and accretion tracers that cannot be contaminated by winds from the literature, it is unlikely that this is the cause of all of the low-lifetime disks we are observing.

4. Unless these objects have extreme variability, the outlier disks are on the verge of dissipation. This may be due to efficient radial drift for group II objects that may not be able to trap material in the outer disk like group I disks,

photoevaporation, and/or truncation of the outer disk due to multiplicity, all of which can result in low disk masses.

5. We have no low disk mass, low accretion rate objects in our Herbig Ae/Be sample, highlighting the bias in identifying these objects, which require accretion signatures and infrared excesses to be considered as such. In particular, the inability to measure accretion rates below $\sim 10^{-9}\, M_{\odot}\, \mathrm{yr}^{-1}$ in these spectral types limits our ability to characterize the $\dot{M}$–M_{disk} relationship during the last stages of disk evolution in young, intermediate-mass systems.

Further work is needed to characterize the high accretion rate, low dust mass sample. Future high-resolution ALMA observations of these disks are needed to determine whether they are compact. Additionally, the sample of Herbig Ae/Be systems with ALMA observations should be expanded, which would allow us to determine whether the low inferred disk lifetime objects constitute only a small fraction of Herbig Ae/Be systems or whether this population is substantial. Finally, to better understand disk evolution around intermediate-mass stars, we should also characterize the precursors of Herbig Ae/Be stars, intermediate-mass T Tauri stars, and their descendants, debris disks, to understand how disks move through this plane from formation to dissipation.

Appendix

In this appendix, we compare the $\dot{M}$ and M_{disk} values that we use in this work to previous values in the literature for all of the objects with an inferred disk lifetime of less than 0.01 Myr. In general, we find that high spatial resolution (sub)millimeter observations are needed to properly determine the disk dust masses, especially for targets with nearby companions that may contaminate low-resolution observations.

1. AB Aur.

Guzmán-Díaz et al. (2021) found that AB Aur has a disk mass of $0.009 \pm 0.002\, M_{\odot}$, assuming a gas-to-dust ratio of 100, using a variety of (sub)millimeter observations. This is within a factor of 3 of our value of $0.0035\, M_{\odot}$ ($M_{\mathrm{dust}} = 11.8\, M_{\oplus}$). Rivière-Marichalar et al. (2022) found that the gas-to-dust mass ratio varies in the disk of AB Aur from $\sim$10 to 40. Therefore, the disk mass is likely to be lower than what we use here, resulting in an even lower disk lifetime than we infer.

There are several values of the accretion rate for AB Aur in the literature: $\log_{10}(\dot{M}) = -6.85$ ($M_{\odot}\, \mathrm{yr}^{-1}$) (Garcia Lopez et al. 2006), $\log_{10}(\dot{M}) = -7.74$ ($M_{\odot}\, \mathrm{yr}^{-1}$) (Donehew & Brittain 2011), $\log_{10}(\dot{M}) = -6.90$ ($M_{\odot}\, \mathrm{yr}^{-1}$) (Salyk et al. 2013), and $\log_{10}(\dot{M}) = -6.13$ ($M_{\odot}\, \mathrm{yr}^{-1}$) (Wichittanakom et al. 2020). We adopt the value from Wichittanakom et al. (2020).

2. HD 104237.

Guzmán-Díaz et al. (2021) found a disk mass of $0.008 \pm 0.002\, M_{\odot}$ for HD 104237, a factor of less than 3 larger than our value of $0.003\, M_{\odot}$ ($M_{\mathrm{dust}} = 10.5\, M_{\oplus}$). The Guzmán-Díaz et al. (2021) disk mass is based on 1.27 mm observations from Henning et al. (1994) using the 15 m SEST telescope with a resolution of $23''$, which would contain several additional sources in the beam. The ALMA observations are not high enough resolution to resolve the disk, but a companion is observed in the continuum, indicating that we are resolving out some, if not all, sources of additional contamination. Kama et al. (2020), using HD observations from Herschel/PACS observations, found a gas-to-dust mass ratio of $\leqslant 300$. Object HD 104237 hosts a binary pair at the center of the circumbinary disk. This has resulted in interesting work on the nature of the inner disk in this system. Garcia et al. (2013) found that Brγ is variable, with the line equivalent width changing by a factor of 2 depending on the binary interaction; however, Garcia Lopez et al. (2006) found an accretion rate of $\log_{10}(\dot{M}) = -7.45$ ($M_{\odot}\, \mathrm{yr}^{-1}$), 1 order of magnitude lower than the value we use here.

3. HD 37258.

Van Terwisga et al. (2022) found a dust mass of $8.9 \pm 0.41\, M_{\oplus}$ for HD 37258 relative to the one derived by Stapper et al. (2022) of $2.4 \pm 0.4\, M_{\oplus}$. These measurements are from the same ALMA observations (2019.1.01813.S; PI: S. van Terwisga), but the fluxes derived are slightly different, and the dust temperatures are different, with van Terwisga et al. (2022) assuming $T_{\mathrm{dust}} = 20$ K and Stapper et al. (2022) using $T_{\mathrm{dust}} = 51$ K, derived from the stellar luminosity.

Fairlamb et al. (2015) found an accretion rate of $\log_{10}(\dot{M}) = -6.98$ ($M_{\odot}\, \mathrm{yr}^{-1}$), the same value as found by Grant et al. (2022).

4. BF Ori.

Guzmán-Díaz et al. (2021) reported a disk mass of $0.005 \pm 0.002\, M_{\odot}$ for BF Ori using observations from the IRAM 30 m telescope presented in Natta et al. (1997). This is 15 times higher than our adopted value from ALMA observations of $3.3 \times 10^{-4}\, M_{\odot}$ ($M_{\mathrm{dust}} = 1.1\, M_{\oplus}$). This is due to two factors; the first is that the IRAM observations have a main beamwidth of $11''$, which likely suffers from contamination compared to the ALMA observations, which have a beam of $1''.49 \times 1''.03$. The ALMA observations are still not high enough resolution to resolve the disk, but they are high enough to minimize contamination from nearby objects and cloud contamination. The second contributing factor is the choice of dust temperature, with Guzmán-Díaz et al. (2021) using a temperature of 25 K, and Stapper et al. (2022) using a value of 58 K.

Several works have reported accretion rates for BF Ori: $\log_{10}(\dot{M}) = -7.06$ ($M_{\odot}\, \mathrm{yr}^{-1}$) (Donehew & Brittain 2011), $\log_{10}(\dot{M}) < -8.0$ ($M_{\odot}\, \mathrm{yr}^{-1}$) (Mendigutía et al.

2011), $\log_{10}(\dot{M}) = -6.65$ $(M_\odot\,\mathrm{yr}^{-1})$ (Fairlamb et al. 2015), and $\log_{10}(\dot{M}) = -7.28$ (Grant et al. 2022; adopted here). The Donehew & Brittain (2011), Mendigutía et al. (2011), and Fairlamb et al. (2015) values are all determined using the Balmer excesses, which are 0.22, 0.0, and 0.15 mag for each of those works, respectively. Object BF Ori is known to exhibit UX Ori–type behavior (e.g., Shenavrin et al. 2012), with photometric variability in the visual and infrared; therefore, we adopt the most recent measurement for the accretion rate, which is within the spread of the previous measurements.

5. HR 5999.

Guzmán-Díaz et al. (2021) found a disk mass of $0.008 \pm 2.19 \times 10^{-4}\,M_\odot$ using observations from SCUBA (Sandell et al. 2011) and SMA (Meeus et al. 2012), in comparison to the disk mass we adopt here of $0.0012\,M_\odot$. The derived fluxes are quite similar, with Meeus et al. (2012) deriving a 1.3 mm flux of 34.3 ± 0.9 mJy, and Stapper et al. (2022) deriving a flux of 26.5 mJy. A companion is seen in the ALMA continuum observations that is well resolved from HR 5999. Yen et al. (2018) used ^{13}CO and C^{18}O ALMA observations paired with models from Miotello et al. (2016) to determine a gas mass of $6^{+7.2}_{-3.2} \times 10^{-5}\,M_\odot$ for HR 5999, which is 20 times lower than our estimate from the dust mass. This gas mass value, when taken with an accretion rate of $\log_{10}(\dot{M}) = -6.0$ $(M_\odot\,\mathrm{yr}^{-1})$, results in an inferred disk lifetime of only 60 yr.

Wichittanakom et al. (2020) rederived the accretion rate for HR 5999 from the observations of Fairlamb et al. (2015, 2017) with updated stellar parameters, finding an accretion rate of $\log_{10}(\dot{M}) = -6.0$ $(M_\odot\,\mathrm{yr}^{-1})$, compared to the accretion rate by Fairlamb et al. (2015) of $\log_{10}(\dot{M}) = -6.25$ $(M_\odot\,\mathrm{yr}^{-1})$. We adopt the accretion rate from Wichittanakom et al. (2020).

6. VV Ser.

Guzmán-Díaz et al. (2021) determined a disk mass of $9.54 \times 10^{-4} \pm 2.730 \times 10^{-4}\,M_\odot$ for VV Ser using observations from the Plateau de Bure Interferometer (Alonso-Albi et al. 2008; Boissier et al. 2011) with a beam of $1''7 \times 0''8$ at 1.3 mm. This matches well with our derived disk mass of $6.9 \times 10^{-4}\,M_\odot$ ($2.3\,M_\oplus$ in dust mass). Pontoppidan et al. (2007) found that the mass of the small dust grains is only $\sim 0.03\,M_\oplus$.

Mendigutía et al. (2011) found a Balmer jump (0.54 mag) that is inconsistent with magnetospheric accretion models; however, Donehew & Brittain (2011) found a Balmer jump of 0.16 mag, which is within the range of magnetospheric models run by Mendigutía et al. (2011). Garcia Lopez et al. (2016) found that several H I lines, including Brγ, are variable, with Brγ likely originating in a disk wind. The models used in that work assume an accretion rate of $3.3 \times 10^{-7}\,M_\odot\,\mathrm{yr}^{-1}$. With these discrepant measurements, it is unclear whether the accretion mechanism is variable and magnetospheric accretion is taking place in this object, and if so, how much of the Brγ line is generated from magnetospheric accretion. However, while the accretion mechanism may be unclear, the accretion rate is likely to be high, given the high Balmer jump observed in both Mendigutía et al. (2011) and Donehew & Brittain (2011). We note that Donehew & Brittain (2011) found an accretion rate of

$\log_{10}(\dot{M}) = -7.49$ $(M_\odot\,\mathrm{yr}^{-1})$ but with a pre-Gaia distance and stellar properties. We adopt an upper limit to the accretion rate of $\log_{10}(\dot{M}) < -6.14$ $(M_\odot\,\mathrm{yr}^{-1})$ from Grant et al. (2022) and do not include it in the $\dot{M}$–M_{disk} fits.

7. HD 58647.

Few (sub)millimeter observations of HD 58647 are available in the literature. We consider the ALMA observations (from Program 2018.1.00814.S) with an rms of 0.14 mJy beam^{-1} and a beam of $0''47 \times 0''39$ and the dust mass determination of $1 \pm 0.1\,M_\oplus$ from Stapper et al. (2022) to be robust.

In comparison to the lack of (sub)millimeter observations, HD 58647 has several U-band and near-infrared observations. Mendigutía et al. (2011) used the Balmer discontinuity and found an accretion rate of $\log_{10}(\dot{M}) = -4.84$ $(M_\odot\,\mathrm{yr}^{-1})$ for HD 58647. Using Brγ observations, Brittain et al. (2007) found an accretion rate of $\log_{10}(\dot{M}) = -6.45$ $(M_\odot\,\mathrm{yr}^{-1})$, Ilee et al. (2014) found an accretion rate of $\log_{10}(\dot{M}) = -6.32$ $(M_\odot\,\mathrm{yr}^{-1})$, and Grant et al. (2022) found an accretion rate of $\log_{10}(\dot{M}) = -5.84$ $(M_\odot\,\mathrm{yr}^{-1})$. We adopt the latter in this work.

8. HD 141569.

Miley et al. (2018) found a gas mass of $6 \times 10^{-4}\,M_\odot$ for HD 141569 using ALMA ^{13}CO (2–1) observations, a factor of 6 above our inferred disk mass of $1 \times 10^{-4}\,M_\odot$. This higher disk mass is still low enough that the inferred disk lifetime is only 0.03 Myr. Guzmán-Díaz et al. (2021) found a disk mass of $1.46 \times 10^{-4}\,M_\odot$ for HD 141569 from millimeter observations, in good agreement with the value that we adopt from Stapper et al. (2022).

For HD 141569, several accretion rates have been determined in the literature: Garcia Lopez et al. (2006) found an accretion rate of $\log_{10}(\dot{M}) = -8.37$ $(M_\odot\,\mathrm{yr}^{-1})$, Mendigutía et al. (2012) found a value of $\log_{10}(\dot{M}) = -6.89$ $(M_\odot\,\mathrm{yr}^{-1})$, and Fairlamb et al. (2015) found a value of $\log_{10}(\dot{M}) = -7.65$ $(M_\odot\,\mathrm{yr}^{-1})$. Grant et al. (2022) and Wichittanakom et al. (2020) updated the value from Fairlamb et al. (2015) to $\log_{10}(\dot{M}) = -7.76$ and -7.23 $(M_\odot\,\mathrm{yr}^{-1})$, respectively. We adopt the value from Grant et al. (2022).

9. HD 9672.

Moór et al. (2019) found a CO gas mass of $1.11 \times 10^{-2}\,M_\oplus$ ($3.33 \times 10^{-8}\,M_\odot$) for HD 9672/49 Cet; however, CO may not be a good tracer of the total disk mass, in particular depending on the gas origin (e.g., Moór et al. 2019). Using the dust continuum and assuming a gas-to-dust mass ratio of 100, Guzmán-Díaz et al. (2021) found a disk mass of $2.92 \times 10^{-4}\,M_\odot$ from infrared photometry from Herschel/PACS, a factor of 7 higher than our value of $3.9 \times 10^{-5}\,M_\odot$. The ALMA observations analyzed in Stapper et al. (2022) should provide a more accurate estimate of the dust mass due to the longer-wavelength observations.

The accretion rate of $\log_{10}(\dot{M}) = -7.80$ $(M_\odot\,\mathrm{yr}^{-1})$ for HD 9672 comes from Wichittanakom et al. (2020), derived from the Fiber-fed Extended Range Optical Spectrograph (Kaufer et al. 1999) spectra from ESO Program 082.A-9011(A).

10. TY CrA.

Cazzoletti et al. (2019) found a dust mass for TY CrA of $0.66\,M_\oplus$ (disk mass of $2 \times 10^{-4}\,M_\odot$, assuming a

gas-to-dust mass ratio of 100), compared to that derived by Stapper et al. (2022) of $0.1\,M_\oplus$ (disk mass of $3 \times 10^{-5}\,M_\odot$, assuming a gas-to-dust mass ratio of 100), from the same data set, largely due to the difference in dust temperature assumed. Guzmán-Díaz et al. (2021) found a disk mass of less than $0.017\,M_\odot$ from the upper limits on the millimeter flux from Henning et al. (1994) and Pezzuto et al. (1997).

The only accretion rate in the literature that we found is that of Garcia Lopez et al. (2006), who found an accretion rate of $\log_{10}(\dot{M}) < -8.31$ $(M_\odot\,\mathrm{yr}^{-1})$ based on the depth of the Brγ line, which indicated little or no accretion taking place in this object.

11. HD 176386. Object

HD 176386 is undetected in the ALMA observation, with the continuum only present at the 1.6σ level (Stapper et al. 2022). That observation had an rms of $0.20\,\mathrm{mJy\,beam^{-1}}$, meaning an upper limit for the flux of $0.32\,\mathrm{mJy}$, corresponding to a dust mass of $0.06\,M_\oplus$ ($1.8 \times 10^{-5}\,M_\odot$ in total disk mass assuming a gas-to-dust ratio of 100). Guzmán-Díaz et al. (2021) used submillimeter observations from SCUBA (Di Francesco et al. 2008) to determine a disk mass of $0.121 \pm 0.01\,M_\odot$. This nearly 4 orders of magnitude difference is due to contamination in the SCUBA maps, which have a $14''$ FWHM in the $850\,\mu\mathrm{m}$ map used. Object HD 176386B is a binary companion to HD 176386 with a separation of $3''7$ (Wilking et al. 1997) and would have contributed to the flux observed in the low-resolution SCUBA observations. The high-resolution ALMA observations, with a beam of $0''43 \times 0''32$, are able to spatially distinguish the sources. Object

HD 176386 has several accretion rates in the literature. Garcia Lopez et al. (2006) found an accretion rate of $\log_{10}(\dot{M}) = -8.11$ $(M_\odot\,\mathrm{yr}^{-1})$, Wichittanakom et al. (2020) found a value of $\log_{10}(\dot{M}) = -7.08$ $(M_\odot\,\mathrm{yr}^{-1})$, and Guzmán-Díaz et al. (2021) found a value of $\log_{10}(\dot{M}) = -6.49$ $(M_\odot\,\mathrm{yr}^{-1})$. Pogodin et al. (2012), whose X-Shooter data are the source of the Hα equivalent width used in Wichittanakom et al. (2020), concluded that magnetospheric accretion cannot be applied to this object, given that the disk may be dispersed. Given that we have stringent upper limits on the disk mass for this object, we agree that the disk may be dispersed, and the accretion rate should be considered with caution. However, the Pogodin et al. (2012) absorption Hα profile for HD 176386 does show shallowing relative to a photospheric model, which may be due to accretion. We take the adapted value from Wichittanakom et al. (2020); however, this value should be used with caution.

12. HD 53367.

The ALMA observations analyzed in Stapper et al. (2022; from Program 2018.1.00814.S) show that HD 53367 is only present in the continuum at the 2.4σ level with an rms of $0.14\,\mathrm{mJy\,beam^{-1}}$. We are not aware of other (sub)millimeter observations of this target.

Donehew & Brittain (2011) found an accretion rate of $\log_{10}(\dot{M}) < -7.92$ $(M_\odot\,\mathrm{yr}^{-1})$ from a Balmer discontinuity of <0.09 mag. Fairlamb et al. (2015) found a similar Balmer discontinuity of 0.10 mag, and they were unable to determine an accretion rate for this source given the very high stellar effective temperature of

$29{,}500 \pm 1000$ K. The $\dot{M}$ value that we adopt here of $\log_{10}(\dot{M}) = -6.97$ $(M_\odot\,\mathrm{yr}^{-1})$ is from Grant et al. (2022), based on strong Brγ line emission. However, given the high stellar mass and effective temperature of this object, this accretion rate should be viewed with caution. Given the low dust mass of this object, if any accretion is taking place, the disk would likely be depleted very quickly.

ORCID iDs

Sierra L. Grant ⬤ https://orcid.org/0000-0002-4022-4899
Lucas M. Stapper ⬤ https://orcid.org/0000-0001-9524-3408
Michiel R. Hogerheijde ⬤ https://orcid.org/0000-0001-5217-537X
Ewine F. van Dishoeck ⬤ https://orcid.org/0000-0001-7591-1907
Sean Brittain ⬤ https://orcid.org/0000-0001-5638-1330
Miguel Vioque ⬤ https://orcid.org/0000-0002-4147-3846

References

Alonso-Albi, T., Fuente, A., Bachiller, R., et al. 2008, ApJ, 680, 1289
Andrews, S. M., Rosenfeld, K. A., Kraus, A. L., & Wilner, D. J. 2013, ApJ, 771, 129
Ansdell, M., Williams, J. P., Manara, C. F., et al. 2017, AJ, 153, 240
Augereau, J. C., & Papaloizou, J. C. B. 2004, A&A, 414, 1153
Baines, D., Oudmaijer, R. D., Porter, J. M., & Pozzo, M. 2006, MNRAS, 367, 737
Banzatti, A., Garufi, A., Kama, M., et al. 2018, A&A, 609, L2
Beckwith, S. V. W., Sargent, A. I., Chini, R. S., & Guesten, R. 1990, AJ, 99, 924
Boehler, Y., Weaver, E., Isella, A., et al. 2017, ApJ, 840, 60
Boersma, C., Peeters, E., Martín-Hernández, N. L., et al. 2009, A&A, 502, 175
Boissier, J., Alonso-Albi, T., Fuente, A., et al. 2011, A&A, 531, A50
Booth, A. S., Walsh, C., Ilee, J. D., et al. 2019, ApJL, 882, L31
Brittain, S. D., Kamp, I., Meeus, G., Oudmaijer, R. D., & Waters, L. B. F. M. 2023, SSRv, 219, 7
Brittain, S. D., Simon, T., Najita, J. R., & Rettig, T. W. 2007, ApJ, 659, 685
Cauley, P. W., & Johns-Krull, C. M. 2014, ApJ, 797, 112
Cazzoletti, P., Manara, C. F., Baobab Liu, H., et al. 2019, A&A, 626, A11
Claes, R. A. B., Manara, C. F., Garcia-Lopez, R., et al. 2022, A&A, 664, L7
Di Folco, E., Péricaud, J., Dutrey, A., et al. 2020, A&A, 635, A94
Di Francesco, J., Johnstone, D., Kirk, H., MacKenzie, T., & Ledwosinska, E. 2008, ApJS, 175, 277
Donehew, B., & Brittain, S. 2011, AJ, 141, 46
Eisner, J. A., Arce, H. G., Ballering, N. P., et al. 2018, ApJ, 860, 77
Fairlamb, J. R., Oudmaijer, R. D., Mendigutía, I., Ilee, J. D., & van den Ancker, M. E. 2015, MNRAS, 453, 976
Fairlamb, J. R., Oudmaijer, R. D., Mendigutia, I., Ilee, J. D., & van den Ancker, M. E. 2017, MNRAS, 464, 4721
Fiorellino, E., Tychoniec, Ł., Manara, C. F., et al. 2022, ApJL, 937, L9
Fischer, W. J., Hillenbrand, L. A., Herczeg, G. J., et al. 2023, in ASP Conf. Ser. 534, Protostars and Planets VII, ed. S. Inutsuka (San Francisco, CA: ASP)
Garcia Lopez, R., Kurosawa, R., Caratti o Garatti, A., et al. 2016, MNRAS, 456, 156
Garcia Lopez, R., Natta, A., Testi, L., & Habart, E. 2006, A&A, 459, 837
Garcia, P. J. V., Benisty, M., Dougados, C., et al. 2013, MNRAS, 430, 1839
Garufi, A., Meeus, G., Benisty, M., et al. 2017, A&A, 603, A21
Grant, S. L., Espaillat, C. C., Brittain, S., Scott-Joseph, C., & Calvet, N. 2022, ApJ, 926, 229
Grant, S. L., Espaillat, C. C., Wendeborn, J., et al. 2021, ApJ, 913, 123
Gravity Collaboration, Ganci, V., Labadie, L., et al. 2021, A&A, 655, A112
Guzmán-Díaz, J., Mendigutía, I., Montesinos, B., et al. 2021, A&A, 650, A182
Guzmán-Díaz, J., Montesinos, B., Mendigutía, I., et al. 2023, A&A, 671, A140
Hartmann, L., Calvet, N., Gullbring, E., & D'Alessio, P. 1998, ApJ, 495, 385
Henning, T., Launhardt, R., Steinacker, J., & Thamm, E. 1994, A&A, 291, 546
Herbig, G. H. 1960, ApJS, 4, 337
Higuchi, A. E., Kóspál, Á., Moór, A., Nomura, H., & Yamamoto, S. 2020, ApJ, 905, 122
Hone, E., Kraus, S., Davies, C. L., et al. 2019, A&A, 623, A38
Iglesias, D. P., Panić, O., van den Ancker, M., et al. 2023, MNRAS, 519, 3958
Ilee, J. D., Fairlamb, J., Oudmaijer, R. D., et al. 2014, MNRAS, 445, 3723

Johnson, J. A., Aller, K. M., Howard, A. W., & Crepp, J. R. 2010, PASP, 122, 905

Joner, M. D., & Hintz, E. G. 2015, AJ, 150, 204

Jones, M. G., Pringle, J. E., & Alexander, R. D. 2012, MNRAS, 419, 925

Kama, M., Folsom, C. P., & Pinilla, P. 2015, A&A, 582, L10

Kama, M., Trapman, L., Fedele, D., et al. 2020, A&A, 634, A88

Kaufer, A., Stahl, O., Tubbesing, S., et al. 1999, Msngr, 95, 8

Kelly, B. C. 2007, ApJ, 665, 1489

Kraus, S., Hofmann, K. H., Benisty, M., et al. 2008, A&A, 489, 1157

Kurosawa, R., Kreplin, A., Weigelt, G., et al. 2016, MNRAS, 457, 2236

Leinert, C., Richichi, A., & Haas, M. 1997, A&A, 318, 472

Liu, Y., Linz, H., Fang, M., et al. 2022, A&A, 668, A175

Lodato, G., Scardoni, C. E., Manara, C. F., & Testi, L. 2017, MNRAS, 472, 4700

Maaskant, K. M., Honda, M., Waters, L. B. F. M., et al. 2013, A&A, 555, A64

Manara, C. F., Ansdell, M., Rosotti, G. P., et al. 2023, in ASP Conf. Ser. 534, Protostars and Planets VII, ed. S. Inutsuka et al. (San Francisco, CA: ASP), 539

Manara, C. F., Natta, A., Rosotti, G. P., et al. 2020, A&A, 639, A58

Manara, C. F., Rosotti, G., Testi, L., et al. 2016, A&A, 591, L3

Manara, C. F., Tazzari, M., Long, F., et al. 2019, A&A, 628, A95

Mann, R. K., Di Francesco, J., Johnstone, D., et al. 2014, ApJ, 784, 82

Meeus, G., Montesinos, B., Mendigutía, I., et al. 2012, A&A, 544, A78

Meeus, G., Waters, L. B. F. M., Bouwman, J., et al. 2001, A&A, 365, 476

Mendigutía, I., Calvet, N., Montesinos, B., et al. 2011, A&A, 535, A99

Mendigutía, I., Mora, A., Montesinos, B., et al. 2012, A&A, 543, A59

Mendigutía, I., Oudmaijer, R. D., Rigliaco, E., et al. 2015, MNRAS, 452, 2837

Miley, J. M., Panić, O., Wyatt, M., & Kennedy, G. M. 2018, A&A, 615, L10

Miotello, A., Kamp, I., Birnstiel, T., Cleeves, L. I., & Kataoka, A. 2023, in ASP Conf. Ser. 534, Protostars and Planets VII, ed. S. Inutsuka et al. (San Francisco, CA: ASP) 501

Miotello, A., van Dishoeck, E. F., Kama, M., & Bruderer, S. 2016, A&A, 594, A85

Mooley, K., Hillenbrand, L., Rebull, L., Padgett, D., & Knapp, G. 2013, ApJ, 771, 110

Moór, A., Kral, Q., Ábrahám, P., et al. 2019, ApJ, 884, 108

Mulders, G. D., Pascucci, I., Manara, C. F., et al. 2017, ApJ, 847, 31

Natta, A., Grinin, V. P., Mannings, V., & Ungerechts, H. 1997, ApJ, 491, 885

Panić, O., Haworth, T. J., Petr-Gotzens, M. G., et al. 2021, MNRAS, 501, 4317

Pezzuto, S., Strafella, F., & Lorenzetti, D. 1997, ApJ, 485, 290

Pogodin, M. A., Hubrig, S., Yudin, R. V., et al. 2012, AN, 333, 594

Pontoppidan, K. M., Dullemond, C. P., Blake, G. A., et al. 2007, ApJ, 656, 980

Reffert, S., Bergmann, C., Quirrenbach, A., Trifonov, T., & Künstler, A. 2015, A&A, 574, A116

Rivière-Marichalar, P., Fuente, A., Esplugues, G., et al. 2022, A&A, 665, A61

Rosotti, G. P., & Clarke, C. J. 2018, MNRAS, 473, 5630

Rosotti, G. P., Clarke, C. J., Manara, C. F., & Facchini, S. 2017, MNRAS, 468, 1631

Salyk, C., Herczeg, G. J., Brown, J. M., et al. 2013, ApJ, 769, 21

Sandell, G., Weintraub, D. A., & Hamidouche, M. 2011, ApJ, 727, 26

Sellek, A. D., Booth, R. A., & Clarke, C. J. 2020, MNRAS, 498, 2845

Shenavrin, V. I., Grinin, V. P., Rostopchina-Shakhovskaja, A. N., Demidova, T. V., & Shakhovskoi, D. N. 2012, ARep, 56, 379

Sicilia-Aguilar, A., Banzatti, A., Carmona, A., et al. 2016, PASA, 33, e059

Stapper, L. M., Hogerheijde, M. R., van Dishoeck, E. F., & Mentel, R. 2022, A&A, 658, A112

Stelzer, B., Robrade, J., Schmitt, J. H. M. M., & Bouvier, J. 2009, A&A, 493, 1109

Tabone, B., Rosotti, G. P., Lodato, G., et al. 2022, MNRAS, 512, L74

Testi, L., Natta, A., Manara, C. F., et al. 2022, A&A, 663, A98

The, P. S., de Winter, D., & Perez, M. R. 1994, A&AS, 104, 315

Toci, C., Rosotti, G., Lodato, G., Testi, L., & Trapman, L. 2021, MNRAS, 507, 818

Trapman, L., Facchini, S., Hogerheijde, M. R., van Dishoeck, E. F., & Bruderer, S. 2019, A&A, 629, A79

van Boekel, R., Min, M., Waters, L. B. F. M., et al. 2005, A&A, 437, 189

van der Marel, N., Cazzoletti, P., Pinilla, P., & Garufi, A. 2016, ApJ, 832, 178

van der Marel, N., & Mulders, G. D. 2021, AJ, 162, 28

van Terwisga, S. E., Hacar, A., van Dishoeck, E. F., Oonk, R., & Portegies Zwart, S. 2022, A&A, 661, A53

Vaňko, M., Eiff, M. A.-V., Pribulla, T., et al. 2013, MNRAS, 431, 2230

Vink, J. S., Drew, J. E., Harries, T. J., & Oudmaijer, R. D. 2002, MNRAS, 337, 356

Vioque, M., Oudmaijer, D., Baines, R., Mendigutía, D., & Pérez-Martínez, R, I. 2018, A&A, 620, A128

Vioque, M., Oudmaijer, R. D., Wichittanakom, C., et al. 2022, ApJ, 930, 39

Virtanen, P., Gommers, R., Oliphant, T. E., et al. 2020, NatMe, 17, 261

Wheelwright, H. E., Oudmaijer, R. D., & Goodwin, S. P. 2010, MNRAS, 401, 1199

Wichittanakom, C., Oudmaijer, R. D., Fairlamb, J. R., et al. 2020, MNRAS, 493, 234

Wilking, B. A., McCaughrean, M. J., Burton, M. G., et al. 1997, AJ, 114, 2029

Winter, A. J., Clarke, C. J., Rosotti, G., et al. 2018, MNRAS, 478, 2700

Wojtczak, J. A., Labadie, L., Perraut, K., et al. 2023, A&A, 669, A59

Yen, H.-W., Koch, P. M., Manara, C. F., Miotello, A., & Testi, L. 2018, A&A, 616, A100

Zagaria, F., Clarke, C. J., Rosotti, G. P., & Manara, C. F. 2022, MNRAS, 512, 3538

Zuckerman, B., & Song, I. 2012, ApJ, 758, 77